Received: 23 January 2024 | Revised: 5 March 2024 | Accepted: 25 March 2024

DOI: 10.1096/fj.202400186R

RESEARCH ARTICLE

The FASEB Journal

Xbp1 promotes odontoblastic differentiation through modulating mitochondrial homeostasis

Delan Huang[1] | **Yuanyuan Li**[1] | **Jiahao Han**[1] | **Huanyan Zuo**[1,2] | **Huan Liu**[1,3,4] | **Zhi Chen**[1,2]

[1]State Key Laboratory of Oral & Maxillofacial Reconstruction and Regeneration, Key Laboratory of Oral Biomedicine Ministry of Education, Hubei Key Laboratory of Stomatology, School & Hospital of Stomatology, Wuhan University, Wuhan, China

[2]Department of Cariology and Endodontics, School of Stomatology, Wuhan University, Wuhan, China

[3]Department of Periodontology, School of Stomatology, Wuhan University, Wuhan, China

[4]TaiKang Center for Life and Medical Sciences, Wuhan University, Wuhan, China

Correspondence
Zhi Chen, State Key Laboratory of Oral & Maxillofacial Reconstruction and Regeneration, Key Laboratory of Oral Biomedicine Ministry of Education, Hubei Key Laboratory of Stomatology, Department of Cariology and Endodontics School & Hospital of Stomatology, Wuhan University, Wuhan 430079, China.
Email: zhichen@whu.edu.cn

Huan Liu, State Key Laboratory of Oral & Maxillofacial Reconstruction and Regeneration, Key Laboratory of Oral Biomedicine Ministry of Education, Hubei Key Laboratory of Stomatology, School & Hospital of Stomatology, Wuhan University, Wuhan 430079, China.
Email: liu.huan@whu.edu.cn

Funding information
National Natural Science Foundation of China, Grant/Award Number: 82230029, 82071110, 82071077 and 82270948

Abstract

Odontoblast differentiation depends on the orderly recruitment of transcriptional factors (TFs) in the transcriptional regulatory network. The depletion of crucial TFs disturbs dynamic alteration of the chromatin landscape and gene expression profile, leading to developmental defects. Our previous studies have revealed that the basic leucine zipper (bZIP) TF family is crucial in odontoblastic differentiation, but the function of bZIP TF family member XBP1 is still unknown. Here, we showed the stage-specific expression patterns of the spliced form *Xbp1s* during tooth development. Elevated *Xbp1* expression and nuclear translocation of XBP1S in mesenchymal stem cells (MSCs) were induced by differentiation medium in vitro. Diminution of *Xbp1* expression impaired the odontogenic differentiation potential of MSCs. The further integration of ATAC-seq and RNA-seq identified *Hspa9* as a direct downstream target, an essential mitochondrial chaperonin gene that modulated mitochondrial homeostasis. The amelioration of mitochondrial dysfunction rescued the impaired odontogenic differentiation potential of MSCs caused by the diminution of *Xbp1*. Furthermore, the overexpression of *Hspa9* rescued *Xbp1*-deficient defects in odontoblastic differentiation. Our study illustrates the crucial role of *Xbp1* in odontoblastic differentiation *via* modulating mitochondrial homeostasis and brings evidence to the therapy of mitochondrial diseases caused by genetic defects.

Abbreviations: ATP, adenosine triphosphate; BETA, Binding and Expression Target Analysis; bZIP, basic leucine zipper; CCK-8, Cell Counting Kit-8; DM, differentiation medium; DP, dental papilla; ER, endoplasmic reticulum; FBS, fetal bovine serum; GO, gene ontology; GREAT, Genomic Regions Enrichment of Annotations Tool; HE, Hematoxylin and eosin; IEE, inner enamel epithelium; IRE1α, inositol-requiring enzyme 1a; MAM, mitochondria-associated ER membrane; MMP, mitochondrial membrane potential; MSCs, mesenchymal stem cells; NFRs, nucleosome-free regions; NR, nicotinamide riboside; PFA, paraformaldehyde; ROS, reactive oxygen species; RP, rank product; TEM, transmission electron microscopy; TFs, transcription factors; TM, tunicamycin; UPR^{ER}, unfolded protein response pathway in ER; UPR^{mt}, UPR in mitochondria; XBP1, X-box-binding protein 1.

KEYWORDS
Xbp1, MSCs, odontoblastic differentiation, mitochondrial homeostasis, *Hspa9*

1 | INTRODUCTION

Teeth are crucial organs that impact chewing, pronunciation, and facial aesthetics. Tooth development is initiated by oral epithelium thickening and subsequently mediated by epithelial-mesenchymal interactions involving molecular signaling pathway crosstalk to form tissues such as enamel and dentin.[1,2] Dentinogenesis requires highly organized odontoblast differentiation and mineralization.[1,3] Transcription factors (TFs) are central to transcriptional regulatory networks of odontoblast differentiation.[1] Our group previously revealed that the basic leucine zipper (bZIP) TF family correlated well with dynamic changes in the chromatin landscape during odontoblastic differentiation.[4] Several bZIP family members were verified to have a positive role in odontoblastic differentiation,[4–6] but the detailed mechanism of other members remained elusive.

As a bZIP TF family member, X-box-binding protein 1 (XBP1) has been characterized as a common fate-determining master regulator in mouse multilineage development.[7,8] *Xbp1*-deficient mice displayed embryonic lethality and developmental defects in liver, heart, and exocrine glands.[9–11] *Xbp1* mRNA has unique noncanonical splicing.[12] Briefly, the unspliced *Xbp1* (*Xbp1u*) mRNA is spliced by the activated inositol-requiring enzyme 1a (IRE1α) in endoplasmic reticulum (ER) membrane to generate the ultimate spliced *Xbp1* (*Xbp1s*) mRNA.[13,14] The well-known function of XBP1 is involved in unfolded protein response pathway in ER (UPR^{ER}) under ER stress or secretory burden.[15,16] UPR^{ER} is a conserved signaling pathway to maintain ER homeostasis.[16] Studies have demonstrated that XBP1 regulates ER biogenesis and function, especially in highly secretory cells *via* UPR^{ER} pathway.[17–19] In contrast, a recent study indicated XBP1 functioned *via* direct transcriptional regulation to lineage-determining factors in multilineage development independent of UPR^{ER}.[7] However, much less was known about the detailed mechanism of *Xbp1* in tooth development.

The dynamic coordination of cellular organelles is essential in differentiation and development. Once the homeostasis of organelles is disturbed, the progress of differentiation and development will be hindered.[20–22] Mitochondria are central to the energy supply among cellular organelles and have distinctive dynamics during cell differentiation.[23] Mitochondrial homeostasis comprises multiple aspects, including mitochondrial mass control, fusion and fission, transport and anchoring, and crosstalk with other organelles.[24] The mitochondrial membrane potential (MMP), adenosine triphosphate (ATP) production, and mitochondrial fusion are increased during odontoblastic differentiation, along with the reduction of reactive oxygen species (ROS) generation, indicating the highly active mitochondrial function.[25,26] Inhibition of the mitochondrial respiratory chain or mitochondrial fusion results in severely impairs odontoblastic differentiation progress, implying the essential role of mitochondrial homeostasis.[26] However, the detailed mechanism on how mitochondrial homeostasis regulates odontoblastic differentiation has yet to be elucidated.

In this study, we revealed the dynamic expression pattern of *Xbp1s* at different stages of tooth development in vivo and odontoblastic differentiation in vitro. Lentiviral knockdown of *Xbp1* revealed its crucial role in odontoblastic differentiation. We further combined ATAC-seq and RNA-seq and inferred the downstream target, mitochondrial chaperone protein gene *Hspa9*, closely related to mitochondrial homeostasis. XBP1S modulated transcription of *Hspa9* and mitochondrial homeostasis. In turn, ameliorating mitochondrial dysfunction rescued the impaired odontogenic differentiation caused by *Xbp1* knockdown. The supplementary *Hspa9* expression rescued the deficiency of *Xbp1*-knockdown MSCs in odontoblastic differentiation. Our study provides insight into the function of *Xbp1* and relevant mitochondrial homeostasis in odontoblastic differentiation.

2 | MATERIALS AND METHODS

2.1 | Animals and embryo collection

All animal experiments were approved by the Institutional Animal Care and Use Committee in School and Hospital of Stomatology of Wuhan University (approval no.07922010A). Mouse embryos and neonatal pups were obtained from timed pregnant C57/BL6 females. The heads of the samples were carefully dissected and fixed in 4% paraformaldehyde (PFA) overnight. Then, samples were dehydrated, embedded in paraffin after sufficient decalcification, and prepared into 5-μm thick slices for subsequent experiments.

2.2 | RNAscope *in situ* hybridization and histologic analysis

RNAscope *in situ* hybridization was performed to detect *Xbp1s* mRNA with chromogenic labeling by RNAscope

2.5 HD Reagent Kit-RED (Advanced Cell Diagnostics, CA, USA). Hematoxylin and eosin (HE) staining was used for tissue histological observation.

2.3 | Cell culture and cell treatments

MSCs were isolated from dental papilla of embryonic day 16.5 mice and cultured in DMEM (HyClone, UT, USA) containing 10% fetal bovine serum (FBS) (HyClone, UT, USA) and 1% streptomycin and penicillin at 37°C in 5% CO_2. To overcome the short lifespan of primary MSCs, an immortalized cell line was established as previously described[27] and used in the following loss-of-function experiments as a stable cell model. For odontoblastic differentiation, cells were induced by the differentiation medium (DM) supplemented with 10 mM β-glycerol phosphate (Sigma, MO, USA), 50 mg/mL ascorbic acid (Sigma, MO, USA), and 10 nM dexamethasone (Sigma, MO, USA). Fresh media were replaced every 2 days. For nicotinamide riboside (NR) treatment, cells were treated with different concentrations of NR (MedChemExpress, NJ, USA) in DMSO. DMSO alone served as the negative control. To mimic the ER stress, tunicamycin (TM) (MedChemExpress, NJ, USA) was added to the medium in the final concentration of 1 μg/mL. HEK293T cells were cultured in a complete medium the same as that of MSCs.

2.4 | Total RNA extraction and RT-qPCR

Total RNA was extracted using the RNA Extraction kit (Omega Bio-tek, GA, USA). One microgram total RNA was reverse-transcribed to cDNA using a reverse transcription mix (Vazyme, Nanjing, China). Subsequently, mRNA expression was determined by RT-qPCR with SYBR Green Kit (Vazyme, Nanjing, China). The sequences of primers synthesized by Sangon Biotechnology (Shanghai, China) were shown in Table S1.

2.5 | Western blot analysis

Total proteins were collected using cell lysis buffer (Merck Millipore, Darmstadt, Germany). For cell nucleus/cytoplasm fraction isolation, the nuclear and cytoplasmic protein extraction kit (Beyotime, Shanghai, China) was used. The equal protein of each sample was separated by 10% SDS-PAGE gels after BCA protein quantification (Thermo Fisher Scientific, MA, USA) and was transferred to PVDF membrane (Roche, Mannheim, Germany) for subsequent western blotting. The membranes were incubated with a quick blocking solution (Pumoke Biotech, Wuhan, China), followed by incubation with primary antibodies and corresponding secondary antibodies (Merck Millipore, Darmstadt, Germany). The primary antibodies used were anti-XBP1 (1:1000, NBP1-77681; Novus Biologicals, Littleton, USA), anti-DMP1 (1:1000, 3844; BioVision, CA, USA), anti-DSPP (1:1000, A8413; Abclonal, Wuhan, China), anti-IRE1α (1:1000, ab37073; Abcam, MA, USA), anti-P-IRE1α (1:1000, ab48187; Abcam, MA, USA), anti-BIP (1:1000, 11587-1-AP; Proteintech, Wuhan, China), anti-HSPA9 (1:1000, 14887-1-AP; Proteintech, Wuhan, China), anti-Flag (1:1000, ANT301; Antgene, Wuhan, China), and anti-β-ACTIN-HRP conjugated (1:4000, PMK058M; Pumoke Biotech, Wuhan, China). ECL solution (Pierce Biotech, NY, USA) was used for signal detection.

2.6 | Cell immunofluorescence

After being seeded in coverslips overnight, cells were washed with PBS and fixed by 4% PFA. Then, cells were further permeabilized using 0.1% Triton X-100 and blocked with 3% bovine serum albumin. Primary antibody anti-XBP1 (1:200, NBP1-77681; Novus Biologicals, Littleton, USA) was then utilized for incubation at 4°C overnight, followed by incubation of subsequent secondary antibody Alexa fluor 594 goat anti-rabbit (Antgene, Wuhan, China) and DAPI staining. Confocal microscopy (Olympus, Tokyo, Japan) was used to obtain confocal fluorescence images of cells.

2.7 | Lentiviral packaging, concentration, and transfection

For the stable *Xbp1* knockdown cell line establishment, cells were transfected by lentivirus Lenti-GFP-*Xbp1* shRNA (shXbp1) or control lentivirus Lenti-GFP-scrambled shRNA (NC) purchased from GenePharma (Shanghai, China). GFP-positive cells were sorted 72 h after transfection for subsequent experiments.

Lentiviral vector plasmids pCDH-CMV-HSPA9-EF1-GFP (overexpressing *Hspa9* vector) and pCDH-CMV-MCS-EF1-GFP (control vector) were purchased from Genecreate (Wuhan, China). Then, lentiviral vector plasmids were co-transfected with lentiviral packaging plasmids psPAX2 and pMD2.G into HEK293T cells for lentiviral packaging. The lentivirus was concentrated by the lentivirus concentration kit (Biodragon, Beijing, China) for subsequent transfection. Cells were transfected by *Hspa9* overexpression (oeHspa9) lentivirus or control vector (CV) lentivirus according to the experimental design.

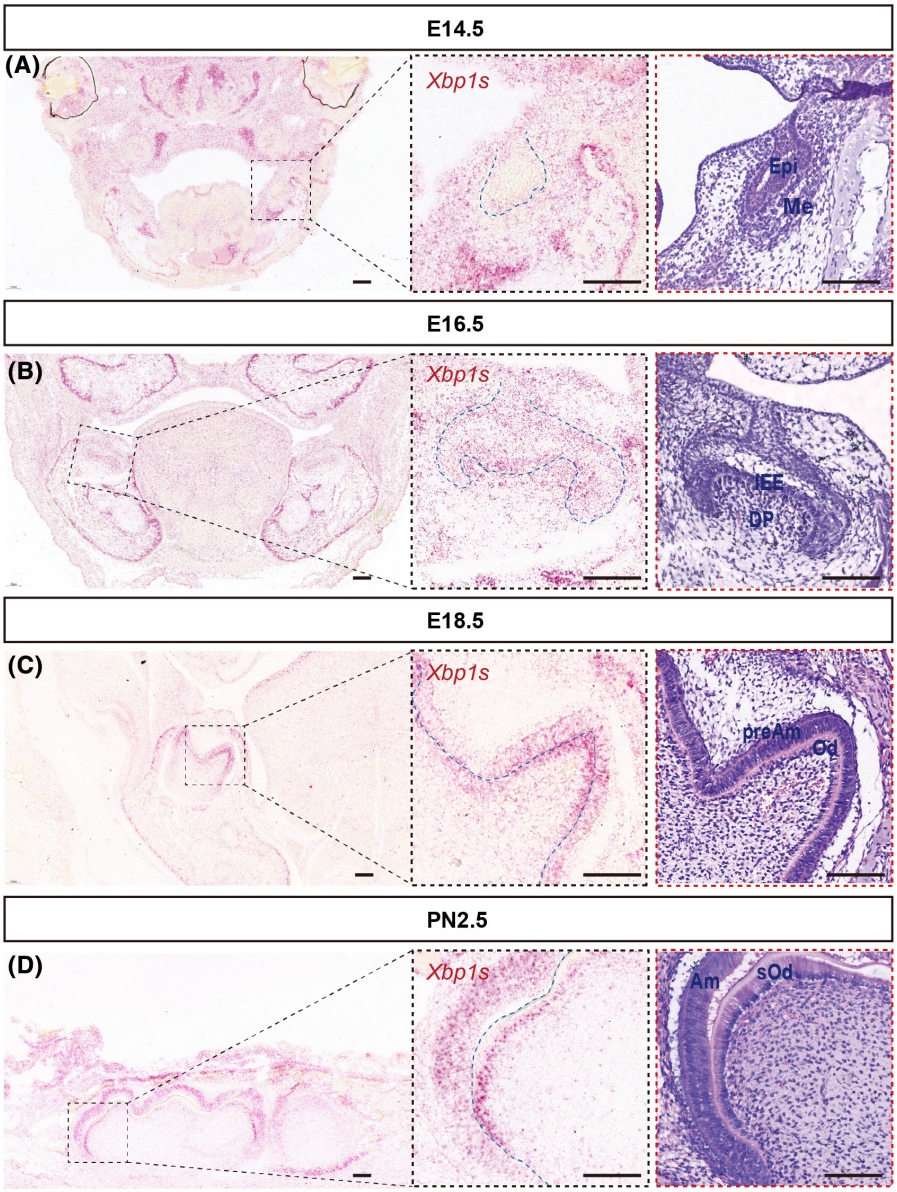

FIGURE 1 The expression pattern of *Xbp1s* during tooth development. (A–D) *In situ* hybridization images of *Xbp1s* mRNA using RNAscope system and the corresponding HE staining images in different development periods of mouse molar. E, embryonic day; PN, postnatal day; Epi, epithelium; Me, mesenchyme; IEE, inner enamel epithelium; DP, dental papilla; preAm, ameloblast precursor cells; Od, odontoblasts; Am, ameloblasts; sOd, secretory odontoblasts. Blue dashed lines indicated the epithelial-mesenchymal border. Scale bar = 100 μm.

2.8 | Alizarin red S staining and semi-quantification

Cells were stained in 1% Alizarin red S solution (Sigma, MO, USA) for 5 min after being fixed by 4% PFA. Then, cells were washed in PBS after staining and photographed by an inverted microscope (Zeiss, Jena, Germany). For semi-quantification, 10% cetylpyridinium chloride (Sigma, MO, USA) was used in a quantitative destaining procedure for Alizarin red S.

FIGURE 2 *Xbp1* expression was increased and peaked at the early period during odontoblastic differentiation of MSCs in vivo and in vitro. (A) *In situ* hybridization images for *Xbp1s* mRNA expression and the corresponding HE staining images in mouse incisor at postnatal day 2.5. Blue dashed lines indicated the epithelial-mesenchymal border. pOd, preodontoblasts; polOd, polarized odontoblasts; sOd, secretory odontoblasts; mOd, mature odontoblasts. Scale bar = 100 μm. (B) The mRNA expression of *Xbp1*, *Xbp1s*, *Dmp1*, and *Dspp* of MSCs in differentiation medium (DM) on Day 0, 1, 3, 5, 7, and 9. (C) The protein expression of *Xbp1*, *Dmp1*, and *Dspp* of MSCs in differentiation medium on Day 0, 1, 3, 5, 7, 9, 11, and 14. (D) The quantitative western blot results on proteins shown in (C). (E) Immunofluorescence staining of XBP1 (red) detected by confocal laser scanning microscope after differentiation induction for 0, 12, and 24 h. Nuclei were visualized by DAPI (blue). Scale bar = 20 μm. (F) The protein expression of *Xbp1* in the cytosol and nucleus isolated from MSCs after differentiation induction for 0, 12, and 24 h. GAPDH and Lamin B1 served as controls for cytoplasmic and nucleus fractions, respectively. (G) The quantitative western blot results on proteins shown in (F). All experiments were performed in triplicate. *$p < .05$, **$p < .01$, ***$p < .001$, ****$p < .0001$ vs. Day 0 or 0 h.

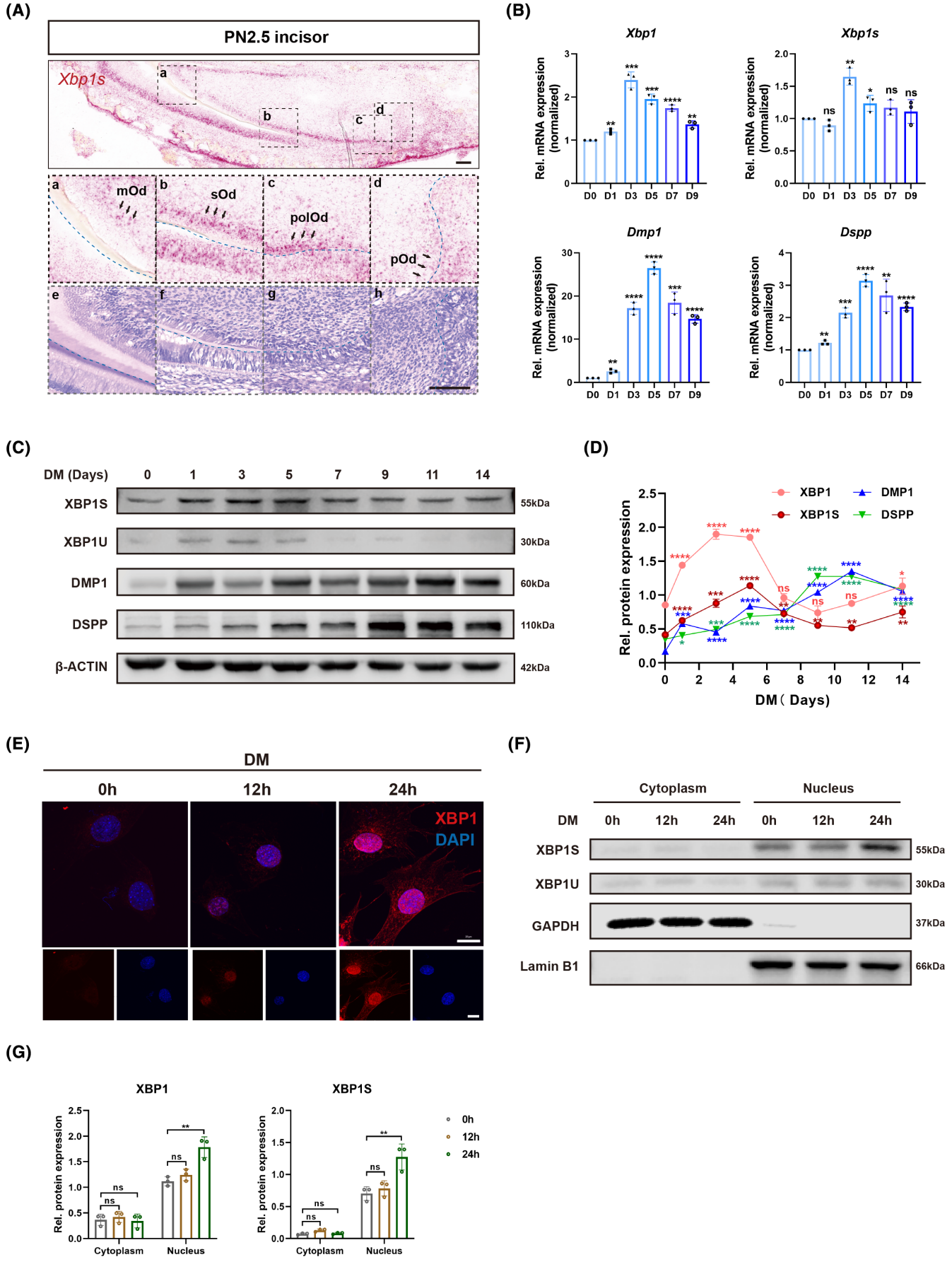
(A)
PN2.5 incisor
Xbp1s
a
b
c
d
mOd
sOd
polOd
pOd
e
f
g
h
(B)
Xbp1
Xbp1s
Dmp1
Dspp
Rel. mRNA expression (normalized)
D0 D1 D3 D5 D7 D9
(C)
DM (Days) 0 1 3 5 7 9 11 14
XBP1S
XBP1U
DMP1
DSPP
β-ACTIN
55kDa
30kDa
60kDa
110kDa
42kDa
(D)
XBP1
XBP1S
DMP1
DSPP
Rel. protein expression
DM（Days)
(E)
DM
0h
12h
24h
XBP1
DAPI
(F)
Cytoplasm
Nucleus
DM 0h 12h 24h 0h 12h 24h
XBP1S
XBP1U
GAPDH
Lamin B1
55kDa
30kDa
37kDa
66kDa
(G)
XBP1
XBP1S
Rel. protein expression
Cytoplasm
Nucleus
0h
12h
24h

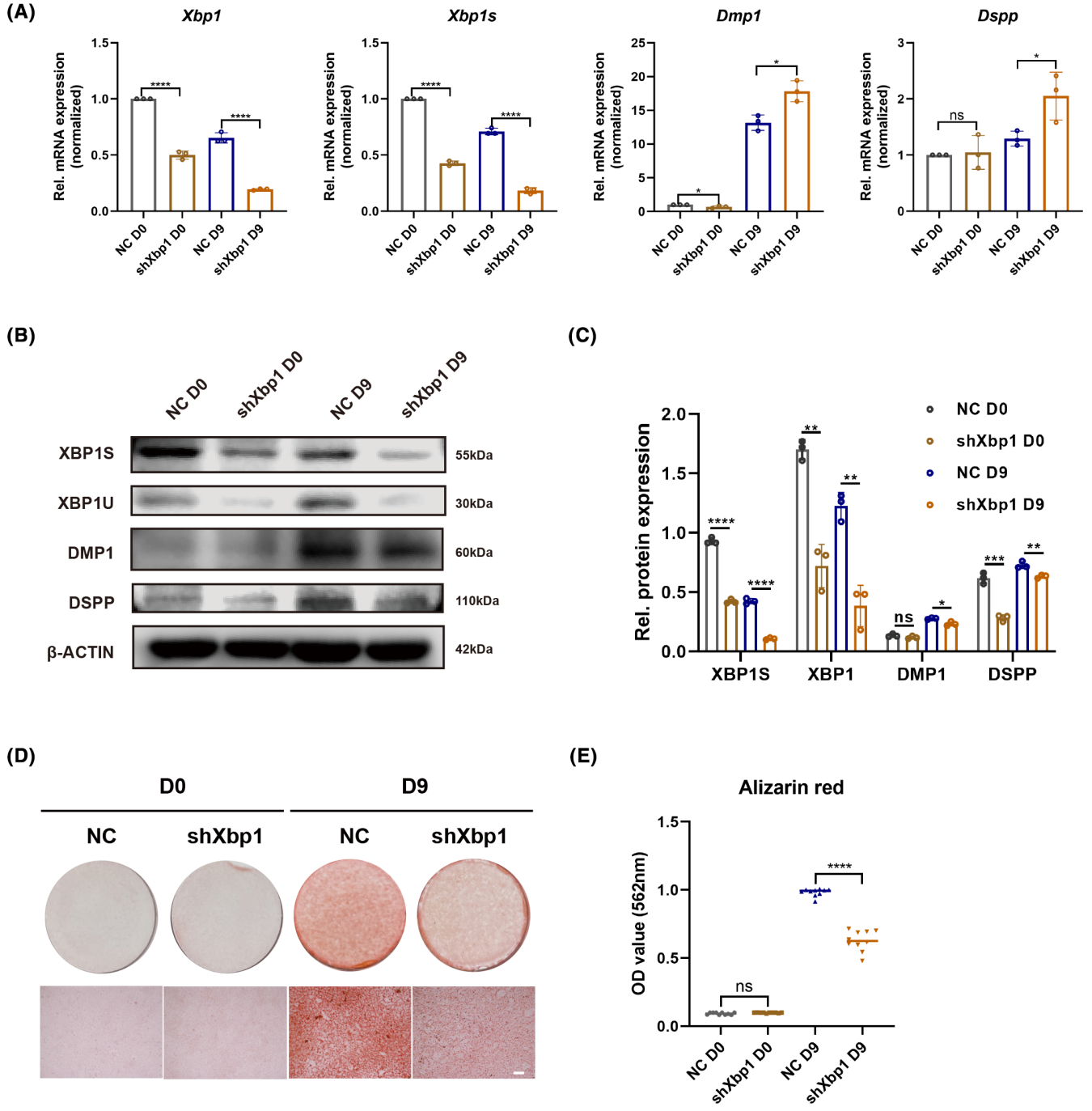

FIGURE 3 *Xbp1* knockdown inhibited odontoblastic differentiation of MSCs in vitro. (A) The mRNA expression of *Xbp1*, *Xbp1s*, *Dmp1*, and *Dspp* in the *Xbp1*-knockdown (shXbp1) group and negative control (NC) group upon differentiation induction on Days 0 and 9. (B) The protein expression of *Xbp1*, *Dmp1*, and *Dspp* in shXbp1 and NC groups upon differentiation induction on Days 0 and 9. (C) The quantitative western blot results on proteins shown in (B). (D) Representative images with Alizarin red S staining after 9-day differentiation induction. The upper were macroscopic images, and the lower were microscopic images. Scale bar = 100 μm. (E) Semi-quantitative evaluation of Alizarin red S staining. All experiments were performed in triplicates. *$p < .05$, **$p < .01$, ***$p < .001$, ****$p < .0001$ vs. NC.

2.9 | ATAC-seq and data analysis

Library preparation and data analysis were done as previously reported.[28,29] Briefly, each group of cells was cultured in differentiation medium for 3 days, and 50 000 cells were used for each library. After the lysis of cell membranes, DNA tagmentation was performed by Tn5 transposase (TD501; Vazyme, Nanjing, China). The DNA library was purified by a purification kit (Qiagen, CA, USA), followed by amplification and indexing with TurePrep™ Index Kit V4 for Illumina (TD204; Vazyme, Nanjing, China). All DNA libraries were cleaned by VAHTS DNA Clean Beads

(Vazyme, Nanjing, China) and sequenced using Illumina Novaseq 6000 (Illumina, CA, USA). After trimming and mapping by trimmomatic v.0.38[30] and bowtie2,[31] PCR duplicates were removed using Picardtools (http://broadinstitute.github.io/picard/). Deeptools2[32] was utilized to generate bigwig files, and MACS2 (v 2.1.1)[33] was applied for peak calling. The bigwig files were uploaded to the UCSC genome browser for visualization. As for the analysis of differentially accessible nucleosome-free regions (NFRs), DiffBind (DESeq2 v.1.26.0)[34] was used, and the result was annotated by Genomic Regions Enrichment of Annotations Tool (GREAT).[35] Homer package was used to identify the motifs enriched in the NFRs of interest and predict direct target regions of XBP1 further.[36] The graphs were plotted with custom R scripts.

2.10 | RNA-seq and data analysis

Total RNA samples were delivered to Wuhan Biobank Co. Ltd (Wuhan, China), for RNA-seq library preparation and analysis. Kallisto (v 0.44.0)[37] was adopted to quantify the abundance of transcripts, and Sleuth R package[38] was used for differential analysis. Gene ontology (GO) enrichment analysis was performed using Metascape[39] and plotted by R scripts.

2.11 | Binding and expression target analysis (BETA)

BETA was a software tool to integrate peak data with transcriptome data for target prediction.[40] Genes were divided into upregulated, downregulated, and unchanged groups. Each gene had its regulatory potential score calculated by peak distribution. Kolmogorov–Smirnov test was used to test the difference between upregulated or downregulated groups with unchanged groups. Direct target prediction was performed by combining nearby peaks and differential expression levels to generate the rank product (RP) value.

2.12 | Plasmid construction

For plasmid construction, *Hspa9* enhancer element was synthesized and cloned into the pGL3-promoter plasmid, and the *Xbp1s* CDS cDNA-3×Flag sequence was synthesized and cloned into the expression plasmid pcDNA3.1 by Genecreate (Wuhan, China). The KOD-Plus-Mutagenesis Kit (Toyobo, Osaka, Japan) was used to generate mutant *Hspa9* enhancer plasmids with different predicted XBP1-binding motif site deletions. Sanger sequencing was performed to validate (Sangon Biotech, Shanghai, China).

2.13 | Luciferase reporter assay

HEK293T cells were seeded in 24-well plates a day in advance. pGL3-promoter-*Hspa9* enhancer, pGL3-promoter-*Hspa9* enhancer-ΔS1, pGL3-promoter-*Hspa9* enhancer-ΔS2, or pGL3-promoter-*Hspa9* enhancer-ΔS3 were co-transfected with pcDNA3.1 or pcDNA3.1-*Xbp1s* CDS-3×Flag by Lipofectamine 2000 reagent (Invitrogen, CA, USA). pRL-TK was used for the normalization of the transfection efficiency. Each group of cells was harvested 48 h after transfection. Dual-Luciferase Reporter Assay System (Promega, WI, USA) and GloMax 20/20 Luminometer (Promega, WI, USA) were applied for luciferase activity detection.

2.14 | CUT&RUN qPCR

CUT&RUN qPCR assay was performed according to the manufacturer's instructions for the Hyperactive pG-MNase CUT&RUN Assay Kit for qPCR (HD101; Vazyme, Nanjing, China). Briefly, cells were collected on Day 3 of in vitro odontoblastic differentiation and incubated with ConA Beads Pro. The cell-bead complex was incubated with anti-XBP1S (1:50, #40435; CST, MA, USA) or rabbit control IgG antibody (1:50, AC005; Abclonal, Wuhan, China) at room temperature for 2 h. After binding with the pG-MNase enzyme, the cell-bead complex was fragmented by $CaCl_2$ solution at 4°C for 2 h. Fragmentation was terminated with a stop buffer. Spike-in DNA was used as a control. The DNA product was isolated, purified, and assayed by qPCR. Agarose gel electrophoresis was performed for the qPCR product verification.

2.15 | Immunohistochemistry

Immunostaining of sections from postnatal day 2.5 mouse incisor were carried out with the diaminobenzidine reagent kit (Maixin, Fuzhou, China). The primary antibody used was anti-HSPA9 (1:200, 14887-1-AP; Proteintech, Wuhan, China). Slides were counterstained with hematoxylin.

2.16 | Mito Deep Red, Mito CMXRos, and MitoSOX assays

Mitochondrial mass, mitochondrial membrane potential, and mitochondrial ROS levels were measured using MitoBright LT Deep Red (Mito Deep Red) (Dojindo Laboratories, Kumamoto, Japan), MitoTracter Red CMXRos (Mito CMXRos) (Invitrogen, CA, USA), and MitoSOX Red mitochondrial superoxide indicator (MitoSOX) (Invitrogen, CA, USA), respectively. Briefly,

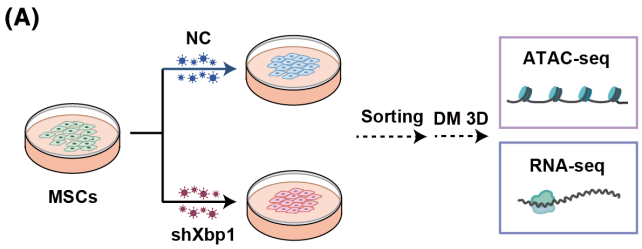

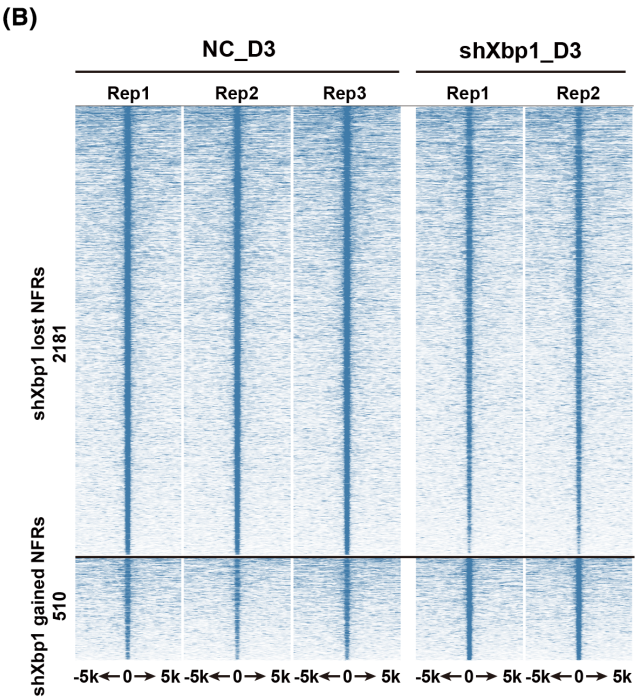

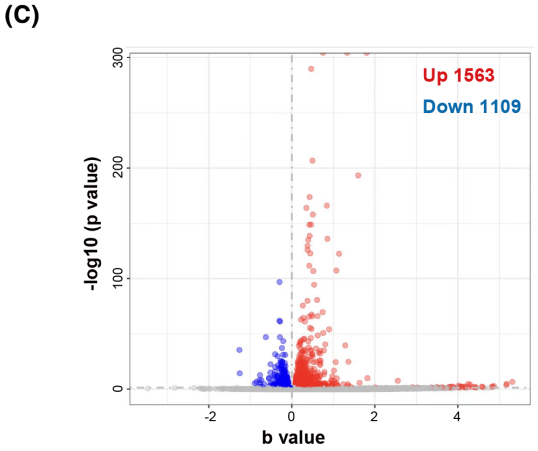

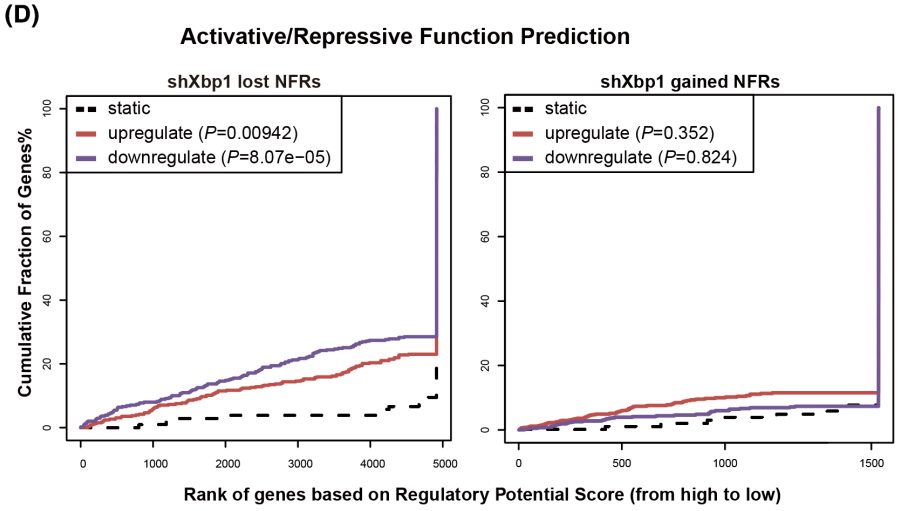

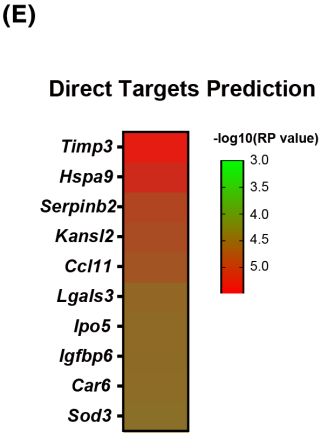

(F)

Enriched TF motifs in shXbp1 lost NFRs

PWM	% of Targets	*P* value	TF family
	50.34%	1e-415	Fra(bZIP)
	53.39%	1e-401	Atf3(bZIP)
	52.24%	1e-382	BATF(bZIP)
	54.23%	1e-368	AP-1(bZIP)
	39.30%	1e-79	RUNX
	12.73%	1e-38	Atf4(bZIP)

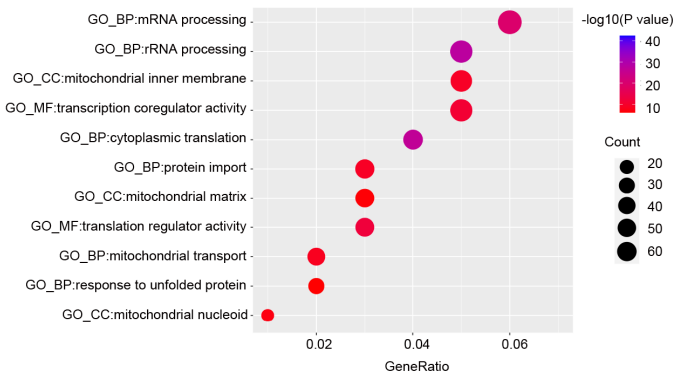

FIGURE 4 *Xbp1* knockdown altered the chromatin landscape and gene expression profile in odontoblastic differentiation. (A) Schematic representation of experimental workflow. (B) Nucleosome-free region (NFR) summit-centered heatmap of ATAC-seq signal in NC_D3 and shXbp1_D3 cells. $n = 2–3$. (C) Volcano plots of bulk RNA-seq data. Red and blue dots represented the upregulated and downregulated genes in shXbp1_D3 cells. $n = 3$. (D) Activative and repressive function prediction results by BETA analysis. The red and violet lines indicated the upregulated and downregulated genes, respectively, whereas the black dotted line indicated genes without differential expression. (E) Top ten predicted direct target genes by BETA analysis. The rank product (RP) values combined the regulatory potential rank with the differential expression changed rank. (F) Top six enriched transcription factor (TF) motifs in shXbp1 lost NFRs. PWM, position weighted matrix. (G) Gene ontology (GO) enrichment for the downregulated genes in shXbp1_D3 RNA-seq data.

cells were stained for 30 min in 100 nM Mito Deep Red, 100 nM Mito CMXRos, or 2 μM MitoSOX and rinsed to remove excess dyes. Flow cytometry (BD Biosciences, CA, USA) was performed for quantitative analysis and further verified by confocal microscopy (Olympus, Tokyo, Japan).

2.17 | Transmission electron microscopy (TEM)

Cells were fixed immediately with 2.5% glutaraldehyde and sent to Servicebio (Wuhan, China) for subsequent processing. The ultrathin sections were prepared and stained following the standard workflow. Images of the respective areas were taken under transmission electron microscopy.

2.18 | SiRNA transfection

SiRNA was designed and synthesized by Genecreate (Wuhan, China). SiRNA sequences were shown in supplemental information. For *Hspa9* knockdown, cells were transfected with *Hspa9* siRNA or negative control siRNA using Lipofectamine 2000 reagent (Invitrogen, CA, USA).

2.19 | Cell counting kit-8 (CCK-8)

Cell viability was analyzed by the CCK-8 kit (Yeasen, Shanghai, China). Cells were seeded in 96-well plates and cultured with appropriate treatments. After 2 h of 10% of CCK-8 solution incubation, optical density values were read at 450 nm using a microplate spectrophotometer (Bio-Tek, Swindon, UK).

2.20 | Quantification of total and secretory proteins

The total and secretory proteins were collected from cell lysate and culture supernatant, respectively, and their volumes were recorded. The protein concentrations were measured and standardized using a BCA Protein Assay Kit (Thermo Fisher Scientific, MA, USA). The protein mass was obtained by multiplying the protein concentration by the volume.

2.21 | ER Tracker assay

ER content was measured using ER Tracker (Beyotime, Shanghai, China). In brief, cells were stained for 30 min and detected by flow cytometry (BD Biosciences, CA, USA) after being rinsed several times.

2.22 | Statistical analyses

One-way ANOVA was applied for multiple group comparisons, and Student *t* test (two-tailed) was applied to compare two groups, except for data analysis of high-throughput sequencing results. $p < 0.05$ was assigned statistical significance.

3 | RESULTS

3.1 | *Xbp1* had a stage-specific expression pattern during tooth development

To thoroughly reveal the expression patterns of the active form of *Xbp1*, namely *Xbp1s*, we performed *in situ* hybridization of the *Xbp1s* mRNA-specific probe at various tooth development stages. At the cap stage (Embryonic day 14.5, E14.5), *Xbp1s* was mainly expressed in osteogenic fronts and barely detected in the whole tooth germ (Figure 1A). The ubiquitous expression of *Xbp1s* was observed at E16.5, the early bell stage (Figure 1B). At this stage, *Xbp1s* was mainly expressed in inner enamel epithelium (IEE) and dental papilla (DP) near the epithelial-mesenchymal border. Moreover, *Xbp1s* was highly expressed in the maxilla and mandible bone area. At E18.5, the late bell stage, IEE cells were differentiated into ameloblast precursor cells, while the adjacent DP cells were differentiated into odontoblasts (Figure 1C). The expression of *Xbp1s* was restricted to the ameloblast precursor cell layer and

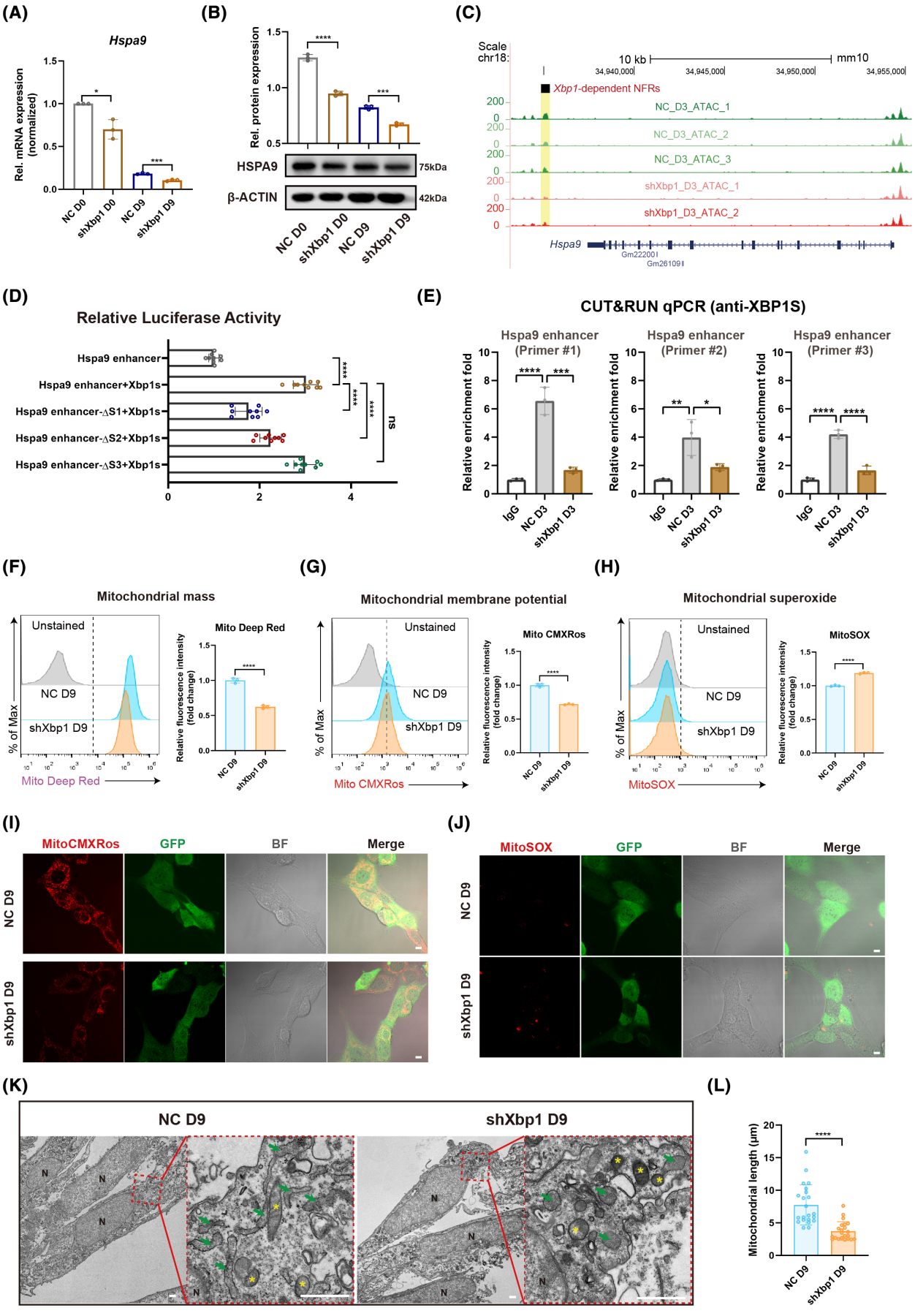
(A)
Hspa9
Rel. mRNA expression (normalized)
NC D0
shXbp1 D0
NC D9
shXbp1 D9
(B)
Rel. protein expression
HSPA9
75kDa
β-ACTIN
42kDa
(C)
Scale
chr18:
10 kb
mm10
Xbp1-dependent NFRs
NC_D3_ATAC_1
NC_D3_ATAC_2
NC_D3_ATAC_3
shXbp1_D3_ATAC_1
shXbp1_D3_ATAC_2
Hspa9
(D)
Relative Luciferase Activity
Hspa9 enhancer
Hspa9 enhancer+Xbp1s
Hspa9 enhancer-ΔS1+Xbp1s
Hspa9 enhancer-ΔS2+Xbp1s
Hspa9 enhancer-ΔS3+Xbp1s
ns
(E)
CUT&RUN qPCR (anti-XBP1S)
Hspa9 enhancer (Primer #1)
Hspa9 enhancer (Primer #2)
Hspa9 enhancer (Primer #3)
Relative enrichment fold
IgG
NC D3
shXbp1 D3
(F)
Mitochondrial mass
Unstained
NC D9
shXbp1 D9
% of Max
Mito Deep Red
Relative fluorescence intensity (fold change)
(G)
Mitochondrial membrane potential
Mito CMXRos
(H)
Mitochondrial superoxide
MitoSOX
(I)
MitoCMXRos
GFP
BF
Merge
(J)
(K)
(L)
Mitochondrial length (μm)

FIGURE 5 XBP1S modulated *Hspa9* transcription and mitochondrial homeostasis in odontoblastic differentiation. (A) The mRNA expression of *Hspa9* in shXbp1 and NC groups upon differentiation induction on Days 0 and 9. (B) The protein expression of *Hspa9* and the quantitative results in shXbp1 and NC groups upon differentiation induction on Days 0 and 9. (C) Visualization of ATAC-seq results at *Hspa9* locus from UCSC genome browser. *Xbp1*-dependent NFRs were shaded in yellow. (D) Dual-luciferase reporter assay results showed the relative enhancer activity of *Hspa9* enhancer reporter with different mutation sites. Luciferase activity was normalized by Renilla luciferase. (E) CUT&RUN qPCR result showed the enrichment of XBP1S signal at *Hspa9* enhancer. (F) Flow cytometry analysis of mitochondrial mass by Mito Deep Red in shXbp1 and NC groups on Day 9. (G, I) Flow cytometry analysis (G) and representative confocal images (I) of mitochondrial membrane potential (MMP)-sensitive Mito CMXRos staining in shXbp1 and NC groups on Day 9. GFP indicated the transfect intensity of lentivirus. BF, bright field. Scale bar = 40 μm. (H, J) Flow cytometry analysis (H) and representative confocal images (J) of mitochondrial reactive oxygen species (ROS) levels by MitoSOX dye in shXbp1 and NC groups on Day 9. GFP indicated the transfect intensity of lentivirus. BF, bright field. Scale bar = 40 μm. (K) Transmission electron microscopy (TEM) representative micrographs of shXbp1 and NC groups on Day 9. Yellow stars indicated mitochondria, and green arrows represented endoplasmic reticulum. N, nucleus. Scale bar = 10 μm. (L) Mitochondrial length measurement in TEM micrographs of shXbp1 and NC groups on Day 9. All experiments were performed in triplicates. *$p < .05$, **$p < .01$, ***$p < .001$, ****$p < .0001$ vs. NC.

odontoblast layer, peaking in the cusps of the odontoblast layer. At the following secretory stage (postnatal day 2.5), the expression of *Xbp1s* in differentiated ameloblasts was markedly elevated, whereas that in tall columnar secretory odontoblasts was decreased (Figure 1D). The stage-specific expression patterns of *Xbp1s* mRNA suggested a unique role of *Xbp1* during tooth development.

3.2 | *Xbp1* expression and nuclear translocation of XBP1S were enhanced during odontoblastic differentiation of MSCs

We further examined the *Xbp1s* mRNA expression in mouse incisor at PN2.5. The result revealed that *Xbp1s* mRNA expression was increased and peaked at the polarized stage of odontoblasts (Figure 2A). A similar expression pattern of *Xbp1* was shown in the tSNE plot of single-cell RNA-seq results which unveiled the odontogenic lineage cells of E18.5 mouse molars (Figure S1A).

During in vitro odontoblastic differentiation of MSCs, the expression of *Xbp1* was gradually increased and peaked at Day 3 in both mRNA and protein levels (Figure 2B–D). The expression pattern of upstream regulator P-IRE1 was consistent with XBP1S, while the expression of ER chaperone BIP, a classical UPR^{ER} downstream of XBP1, was increased continuously during odontoblastic differentiation (Figure S1B,C). Considering the function of XBP1 in active transcriptional regulation, we performed immunofluorescence staining and western blotting of XBP1 at an early period in odontoblastic differentiation, and results showed the enhanced nuclear translocation of XBP1S (Figure 2E–G). XBP1-targeting genes (regulons) were located predominantly in odontoblasts of E18.5 mouse molars, implying the active TF function of XBP1 (Figure S1D).

3.3 | *Xbp1* knockdown impaired the odontoblastic differentiation potential of MSCs

After unveiling the characteristic expression pattern of *Xbp1* during odontoblastic differentiation, we investigated the loss-of-function phenotype of *Xbp1* using the mesenchymal stem cell line established as previously described.[27] Initially, we transferred MSCs with designed RNA interference lentivirus and verified the knockdown efficiency in mRNA and protein levels (Figure 3A–C). After differentiation induction for 0 or 9 days, the expressions of odontogenic markers *Dmp1* and *Dspp* were notably decreased in the protein level despite a slight increase in the mRNA level (Figure 3A–C). Notably, the expression of UPR^{ER} downstream target BIP was unchanged in the shXbp1 group, ruling out the possibility of UPR^{ER} resistance (Figure S2A–D). Alizarin red S staining results and the semi-quantitative analysis indicated that cells in the shXbp1 group formed significantly less mineralized nodules on Day 9, demonstrating the impaired odontoblast differentiation potential of MSCs caused by *Xbp1* knockdown (Figure 3D,E). The results mentioned above implied a positive role of *Xbp1* in odontoblast differentiation independent of UPR^{ER}, but the molecular mechanism underlying the role of *Xbp1* in odontoblast differentiation remains elusive.

3.4 | *Xbp1* knockdown decreased chromatin accessibility and the expression level of gene set associated with mitochondria in odontoblastic differentiation

To further explore the mechanism, we performed ATAC-seq and RNA-seq to reveal the chromatin landscape and gene expression profile of shXbp1 and NC groups during

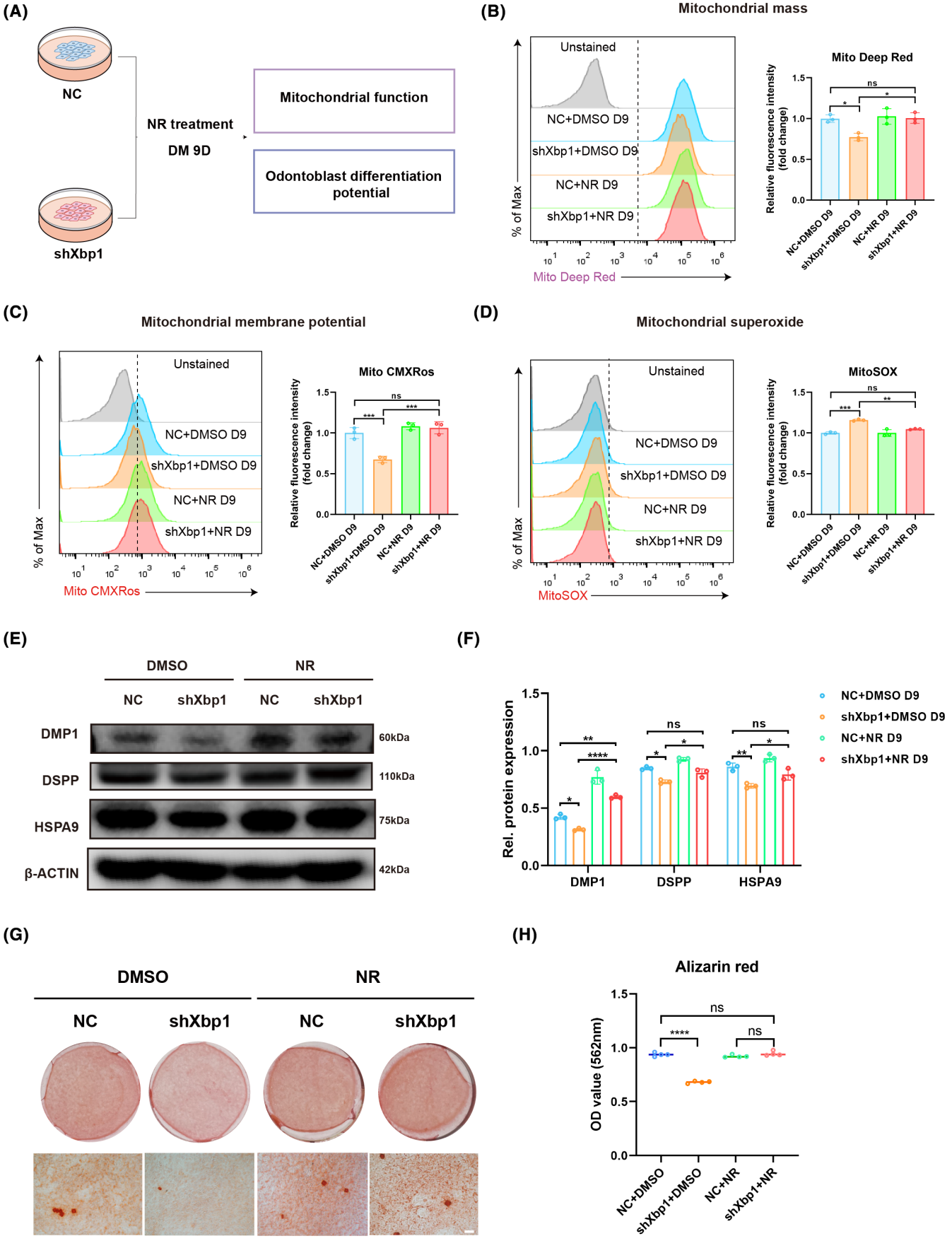
(A)
NC
shXbp1
NR treatment
DM 9D
Mitochondrial function
Odontoblast differentiation potential
(B)
Mitochondrial mass
Unstained
NC+DMSO D9
shXbp1+DMSO D9
NC+NR D9
shXbp1+NR D9
% of Max
Mito Deep Red
Mito Deep Red
Relative fluorescence intensity (fold change)
(C)
Mitochondrial membrane potential
Mito CMXRos
Mito CMXRos
(D)
Mitochondrial superoxide
MitoSOX
MitoSOX
(E)
DMSO
NR
NC
shXbp1
DMP1
DSPP
HSPA9
β-ACTIN
60kDa
110kDa
75kDa
42kDa
(F)
Rel. protein expression
DMP1
DSPP
HSPA9
(G)
DMSO
NR
(H)
Alizarin red
OD value (562nm)
NC+DMSO
shXbp1+DMSO
NC+NR
shXbp1+NR

FIGURE 6 The impaired odontoblastic differentiation capability was rescued by ameliorating *Xbp1* knockdown-induced mitochondrial dysfunction. (A) Schematic representation of experimental workflow. (B) Flow cytometry analysis of mitochondrial mass by Mito Deep Red in shXbp1 and NC groups with or without NR treatment upon differentiation induction on Day 9. (C) Flow cytometry analysis of MMP-sensitive Mito CMXRos staining in shXbp1 and NC groups with or without NR treatment upon differentiation induction on Day 9. (D) Flow cytometry analysis of mitochondrial ROS levels by MitoSOX dye in shXbp1 and NC groups with or without NR treatment upon differentiation induction on Day 9. (E) The protein expression of *Dmp1*, *Dspp*, and *Hspa9* in shXbp1 and NC groups with or without NR treatment upon differentiation induction on Day 9. (F) The quantitative western blot results on proteins shown in (E). (G) Representative images with Alizarin red S staining after 9-day differentiation induction. The upper were macroscopic images, and the lower were microscopic images. Scale bar = 50 μm. (H) Semi-quantitative evaluation of Alizarin red S staining. *$p < .05$, **$p < .01$, ***$p < .001$, ****$p < .0001$ vs. the corresponding group.

odontoblastic differentiation. Our previous study found that the chromatin accessibility associated with bZIP family motifs was most significantly altered on Day 3 of in vitro odontoblastic differentiation[4]; therefore, we performed the high-throughput sequencing on Day 3 (Figure 4A). Analysis of the ATAC-seq atlas showed 2181 regions were enriched in the NC group while 510 regions were enriched in the shXbp1 group, indicating that *Xbp1* knockdown was accompanied by decreased chromatin accessibility during odontoblastic differentiation (Figure 4B). Transcriptome landscapes from RNA-seq data identified 1563 upregulated genes and 1109 downregulated genes (Figure 4C).

We combined the chromatin accessibility landscape with the gene expression profile using BETA analysis.[40] Activative and repressive function prediction results revealed that the downregulated gene set had a much higher regulatory potential score in shXbp1 lost NFRs than other gene sets, consistent with the transcriptional activation function of XBP1 (Figure 4D). The direct target prediction of XBP1 found 56 potential target genes (Table S2), and the top 10 genes were shown in Figure 4E. The motif enrichment analysis of 2181 *Xbp1*-dependent NFRs discovered six highly enriched motifs (Figure 4F). Except for the bZIP motif family, RUNX motif enrichment was the same as in our previous study of several vital TFs in odontoblastic differentiation.[28,29,41]

Gene ontology (GO) enrichment analysis of 2181 *Xbp1*-dependent NFRs using GREAT showed the enrichment in absent teeth and other abnormal developments (Figure S3). Interestingly, downregulated genes were enriched in GO terms, such as mRNA and rRNA processing, transcriptional coregulator activity, and translational regulator activity, indicating relatively decreased transcription and translation levels (Figure 4G). They were also enriched in GO terms associated with mitochondrial homeostasis, such as mitochondrial inner membrane, mitochondrial matrix and mitochondrial nucleoid of cellular component, and mitochondrial transport of biological process (Figure 4G). GO enrichment results suggested that *Xbp1* knockdown impaired cell biological processes and mitochondrial function. We further integrated the predicted target genes with GO enrichment results and found that *Hspa9* was most likely the direct target of XBP1.

3.5 | XBP1S modulated *Hspa9* transcription and mitochondrial homeostasis in odontoblastic differentiation

The mRNA and protein expression levels of predicted target *Hspa9* in the shXbp1 group were significantly decreased following *Xbp1* knockdown on Day 0 and Day 9 of odontoblastic differentiation (Figure 5A,B). In the downstream of the *Hspa9* locus, we noticed that an ATAC-seq peak was markedly decreased in shXbp1 groups, indicating that XBP1 controlled *Hspa9* by directly regulating the associated enhancer (Figure 5C). To detect whether the *Xbp1*-dependent NFRs exert enhancer activity of *Hspa9*, we performed the dual-luciferase reporter assay and chose three bZIP family motifs by the JASPR website as the potential binding motif sites of XBP1S. The results showed the binding motif sites 1 and 2 within *Hspa9* enhancer directly regulated by XBP1S (Figure 5D). The direct regulatory function of XBP1S on *Hspa9* enhancer was further validated by CUT&RUN qPCR. The anti-XBP1S CUT&RUN qPCR result revealed the enrichment of XBP1S signal at one of *Hspa9* enhancers, which was coherent with the analysis of ATAC-seq (Figures 5E and S5). In addition, the *Hspa9* expression showed the same pattern as *Xbp1s* expression during in vivo odontoblastic differentiation, implying the strong link between *Hspa9* and *Xbp1* (Figure S6A).

As a chaperone protein, HSPA9 is actively involved in stabilizing and importing nuclear gene products and refolding mitochondrial precursor proteins.[42,43] It has also been verified as an essential tether protein for mitochondria-associated ER membrane (MAM) formation through the IP3R-GRP75-VDAC1 complex.[44] Various studies have demonstrated that HSPA9 regulated mitochondrial homeostasis, including mitochondrial function, fusion, and MAM formation.[42,44,45] To further unveil the role of *Hspa9* in odontoblastic differentiation,

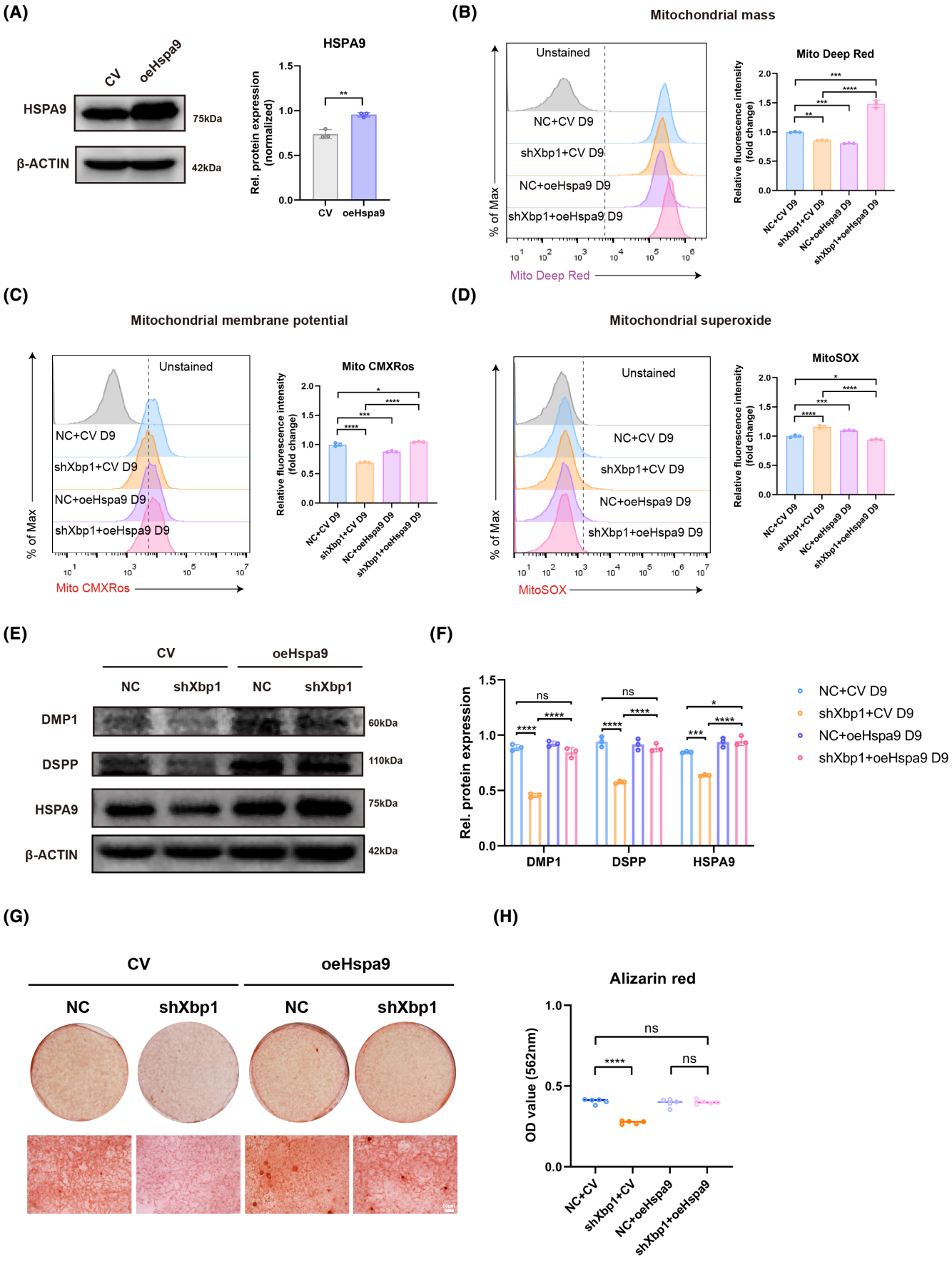
(A)
CV
oeHspa9
HSPA9
β-ACTIN
75kDa
42kDa
HSPA9
Rel. protein expression (normalized)
CV
oeHspa9
(B)
Mitochondrial mass
Unstained
NC+CV D9
shXbp1+CV D9
NC+oeHspa9 D9
shXbp1+oeHspa9 D9
% of Max
Mito Deep Red
Mito Deep Red
Relative fluorescence intensity (fold change)
(C)
Mitochondrial membrane potential
Mito CMXRos
Mito CMXRos
(D)
Mitochondrial superoxide
MitoSOX
MitoSOX
(E)
CV
oeHspa9
NC
shXbp1
DMP1
DSPP
HSPA9
β-ACTIN
60kDa
110kDa
75kDa
42kDa
(F)
Rel. protein expression
DMP1
DSPP
HSPA9
(G)
(H)
Alizarin red
OD value (562nm)
NC+CV
shXbp1+CV
NC+oeHspa9
shXbp1+oeHspa9

FIGURE 7 The impaired phenotype of *Xbp1*-deficient MSCs in odontoblastic differentiation was rescued by overexpressing *Hspa9*. (A) Validation of *Hspa9* overexpression by western blot analysis. (B) Flow cytometry analysis of mitochondrial mass by Mito Deep Red in NC-CV, shXbp1-CV, NC-oeHspa9, and shXbp1-oeHspa9 groups upon differentiation induction on Day 9. (C) Flow cytometry analysis of MMP-sensitive Mito CMXRos staining in each group cells upon differentiation induction on Day 9. (D) Flow cytometry analysis of mitochondrial ROS levels by MitoSOX dye in each group cells upon differentiation induction on Day 9. (E) The protein expression of *Dmp1*, *Dspp*, and *Hspa9* in each group cells upon differentiation induction on Day 9. (F) The quantitative western blot results on proteins shown in (E). (G) Representative images with Alizarin red S staining after 9-day differentiation induction. The upper were macroscopic images, and the lower were microscopic images. Scale bar = 50 μm. (H) Semi-quantitative evaluation of Alizarin red S staining. *$p < .05$, **$p < .01$, ***$p < .001$, ****$p < .0001$ vs. the corresponding group.

we prepared *Hspa9*-knockdown MSCs by *Hspa9* siRNA transfection and chose the most effective one for subsequent experiments (Figure S6B,C). *Hspa9* knockdown led to the decreased expression of DMP1 and DSPP and the impaired formation of calcium nodule on Day 9 (Figure S6D–G).

We measured mitochondrial mass, mitochondrial membrane potential (MMP), and mitochondrial ROS levels in shXbp1 and NC groups after differentiation induction to examine mitochondrial homeostasis (Figure 5F–J). Results showed that the mitochondrial mass and MMP of MSCs in the shXbp1 group were significantly decreased, and the mitochondrial ROS level was significantly increased in the shXbp1 group compared with the NC group, indicating that *Xbp1* knockdown led to mitochondrial dysfunction in MSCs during odontoblast differentiation. Transmission electron microscopy (TEM) observation showed slightly swollen round mitochondria with reduced mitochondrial crista and mitochondrial length in MSCs of the shXbp1 group (Figure 5K,L). Notably, the distance between rough ER and mitochondria was longer, and the rough ER was significantly enlarged. Taken together, results demonstrated that XBP1 modulated mitochondria function, fusion, and MAM formation *via* the transcriptional regulation of *Hspa9* in odontoblastic differentiation.

3.6 | The attenuation of mitochondrial dysfunction rescued the impaired odontoblastic differentiation potential of *Xbp1*-knockdown MSCs

To examine whether mitochondrial dysfunction plays an essential role in the impaired odontoblastic differentiation potential in the shXbp1 group, we used NR as a therapeutic agent[46] to treat cells of the shXbp1 and NC groups, respectively (Figure 6A). We chose 100 μM as the optimum concentration of NR according to the cell activity measurement under NR treatment with different gradient concentrations (Figure S7). After NR treatment, the decreased mitochondrial mass and MMP were upregulated, and the elevated mitochondrial ROS level was reduced in the shXbp1 group, which indicated the attenuation of mitochondrial dysfunction (Figure 6B–D). The protein expression level of *Hspa9* was also recovered by NR treatment simultaneously. The expression levels of specific markers *Dmp1* and *Dspp* were also upregulated by NR treatment in the shXbp1 group after 9-day odontoblastic differentiation (Figure 6E,F). Alizarin red S staining and semi-quantitative evaluation further verified the recovery of odontoblastic differentiation potential in cells of the shXbp1 group (Figure 6G,H). Overall, the attenuation of mitochondrial dysfunction by NR treatment successfully improved the impaired odontoblastic differentiation potential in *Xbp1*-knockdown cells.

3.7 | Overexpression of *Hspa9* rescued the defects of *Xbp1*-deficient MSCs in odontoblastic differentiation

We constructed a lentivirus overexpressing *Hspa9* to rescue *Hspa9* expression in *Xbp1*-knockdown MSCs. The expression efficiency of *Hspa9* overexpression (oeHspa9) lentivirus was verified at the protein level (Figure 7A). After transfection of oeHspa9 lentivirus, the mitochondrial dysfunction of shXbp1 group cells was alleviated, indicated by the upregulated mitochondrial mass and MMP along with the reduced mitochondrial ROS level (Figure 7B–D). Furthermore, the recovery of *Hspa9* expression notably enhanced the DMP1 and DSPP expression of shXbp1 cells and rescued the impaired calcium nodule-forming ability of shXbp1 cells (Figure 7E–H). However, overexpressing *Hspa9* impaired the mitochondrial function of NC cells, implying the dual role of *Hspa9* in mitochondrial homeostasis. Taken together, the sufficient expression of *Hspa9* was crucial in odontoblastic differentiation, especially in *Xbp1*-knockdown MSCs.

4 | DISCUSSION

Transcriptional regulatory network centered on TFs has been extensively involved in cell fate determination during

tooth development.[3] Our study showed that XBP1 was expressed during odontoblastic differentiation and functioned as an active TF, similar to other bZIP family members such as ATF2, ATF5, and ATF6.[4–6] The alterations in chromatin accessibility and transcriptome atlas caused by *Xbp1* knockdown indicated that the odontoblastic differentiation process and the mitochondrial biological activity were disturbed. Mitochondrial quality control regulation was of great importance in the lifetime of organisms, including development and aging.[47,48] Previous studies have shown that odontoblastic differentiation is closely associated with mitochondrial function and dynamics.[25,26] Combining ATAC-seq and RNA-seq data using BETA analysis, we found *Hspa9* to be the direct target gene of XBP1 and verified the direct binding between XBP1S and *Hspa9* enhancer. Published research demonstrated that the perturbed mitochondrial network decreased protein synthesis.[49] Our GO analysis results also showed that downregulated genes in *Xbp1*-knockdown cells were associated with translation attenuation. Additionally, the protein content of cell lysate was decreased in *Xbp1*-knockdown cells after 9-day odontoblastic differentiation (Figure S8A). The slight increase in the mRNA level of *Dmp1* and *Dspp* might attribute to the transcriptional-translational conflict induced by slowing translation.[50]

IRE1α-XBP1 axis is the crucial branch of UPR^{ER}. Under stress, UPR^{ER} predominated in highly secretory cells with well-developed ER, while UPR in mitochondria (UPR^{mt}) was less important.[51,52] UPR^{mt} had a strong link with UPR^{ER}.[52,53] Increasing evidence indicated that some key factors, such as ATF4, ATF5, and CHOP, acted as the crosstalk hubs of UPR^{ER} and UPR^{mt}.[54–56] Mitochondrial chaperones such as HSPA9, proteases such as LONP, antioxidants such as SOD2, and protein import components were the downstream targets of UPR^{mt} pathway.[56] Interestingly, the knockdown of *Xbp1* in MSCs did not downregulate UPR^{ER} pathway, implying that the function of XBP1 in odontoblastic differentiation was independent of UPR^{ER}. We revealed that XBP1 acted as a novel hub between UPR^{ER} and UPR^{mt} pathway via transcriptional regulation of *Hspa9*. UPR^{mt} pathway was involved in odontoblastic differentiation possibly due to the undeveloped ER and high energy demand for differentiation in immature odontoblasts.

Increased expression of *Xbp1* during tooth development can hint at ER stress. Previous studies have demonstrated ER stress was involved in odontogenic differentiation, and ER stress signaling pathways, including UPR^{ER} pathway, were activated during odontogenic differentiation due to the increased secretory demand of ameloblasts and odontoblasts.[57] However, our study revealed that *Xbp1* expression peaked at polarized odontoblasts and then decreased, which was inconsistent with ER stress changes. *Xbp1* knockdown didn't affect ER stress-associated pathways in odontoblastic differentiation. Additionally, the scRNA-seq and high-resolution mass spectrometry study of $Xbp1^{-/-}$ embryos showed canonical *Xbp1* targets related to the UPR^{ER} displayed no significant changes in lineage maturation.[7] All of these results indicated a direct role of *Xbp1* in cell fate determination via transcriptional regulation, which was independent of the UPR^{ER}.

The mitochondrial-ER communication was the crucial regulator in the lineage-specific differentiation of stem cells, which mainly depended on the mechanistic connection between mitochondrial and ER.[20] As the component of mitochondrial-ER contact, HSPA9 controlled ER-mitochondria tethering and their calcium ion transport and further regulated mitochondrial metabolism and ER homeostasis.[58–61] In our study, *Xbp1* knockdown in MSCs led to deficient expression of *Hspa9* during odontoblastic differentiation. For mitochondrial metabolism, the measurement results of mitochondrial mass, MMP, and ROS level illustrated mitochondrial dysfunction caused by *Xbp1* knockdown. Additionally, the mitochondrial-ER contact was attenuated, and the rough ER was enlarged. The ER content and secretory protein level of shXbp1 cells were also reduced, which might be associated with ER homeostasis (Figure S8B,C). However, more evidence was needed for the detailed mechanism of XBP1 and HSPA9 in ER homeostasis during odontoblastic differentiation.

The therapy of primary and secondary mitochondrial diseases characterized by mitochondrial dysfunction was still a clinical conundrum. Recently, UPR^{mt} modulation, such as NR treatment, functioned as a promising therapeutic target already verified in treating mitochondrial diseases such as diabetes, osteoarthritis, and neurodegenerative diseases.[62–64] In our study, we chose NR as the therapeutic reagent for mitochondrial dysfunction in shXbp1 cells, further confirming the recovery of odontoblastic differentiation potential after NR treatment. The deficient expression of *Hspa9* was also increased to a normal level. Our result illustrated that UPR^{mt} modulation provided a novel treatment for mitochondrial diseases caused by genetic defects.

In summary, our study revealed the stage-specific expression pattern of *Xbp1* during tooth development and investigated the positive function of XBP1 during odontoblastic differentiation. XBP1 modulated the chromatin landscape and gene expression profiles in odontoblastic differentiation, primarily regulating mitochondrial homeostasis *via* the transcriptional control of *Hspa9*. Mitochondrial dysfunction in MSCs impaired the odontoblast differentiation potential, and the attenuation of mitochondrial dysfunction successfully rescued the odontoblast differentiation. Furthermore, the rescue of *Hspa9* expression protected the mitochondrial homeostasis and odontoblast differentiation potential of *Xbp1*-deficient

MSCs. Our study provided insight into the function of XBP1 and the dynamic coordination of organelles during odontoblast differentiation.

AUTHOR CONTRIBUTIONS

Delan Huang, Huan Liu, and Zhi Chen designed the experiments. Delan Huang and Yuanyuan Li performed the experiments. Delan Huang, Jiahao Han, and Huanyan Zuo analyzed the data. Delan Huang wrote the manuscript. Huan Liu and Zhi Chen participated in the critical revision of the paper. All authors read and approved the final manuscript.

ACKNOWLEDGMENTS

This work was supported by National Natural Science Foundation of China (Key Program No. 82230029 and 82071110) to Zhi Chen and National Natural Science Foundation of China (No. 82071077 and 82270948) to Huan Liu.

DISCLOSURES

The authors declare no conflicts of interest.

DATA AVAILABILITY STATEMENT

The RNA-seq and ATAC-seq data in our study were available in Genome Sequence Archive (GSA) with the submission ID of CRA013632.

ORCID

Delan Huang https://orcid.org/0000-0003-3763-6195
Yuanyuan Li https://orcid.org/0000-0002-9656-2109
Jiahao Han https://orcid.org/0009-0008-0057-6452
Huanyan Zuo https://orcid.org/0009-0008-2616-5424
Huan Liu https://orcid.org/0000-0002-9947-6687
Zhi Chen https://orcid.org/0000-0003-2095-1324

REFERENCES

1. Kovacs CS, Chaussain C, Osdoby P, Brandi ML, Clarke B, Thakker RV. The role of biomineralization in disorders of skeletal development and tooth formation. *Nat Rev Endocrinol*. 2021;17:336-349.
2. Thesleff I, Sharpe P. Signalling networks regulating dental development. *Mech Dev*. 1997;67:111-123.
3. Yu T, Klein OD. Molecular and cellular mechanisms of tooth development, homeostasis and repair. *Development*. 2020;147:dev184754.
4. Zhang Q, Huang Z, Zuo H, et al. Chromatin accessibility predetermines odontoblast terminal differentiation. *Front Cell Dev Biol*. 2021;9:769193.
5. Zuo H, Xiao Y, Han J, et al. Phosphorylation of ATF2 promotes odontoblastic differentiation via intrinsic HAT activity. *J Genet Genomics*. 2023;50:497-510.
6. Kim JW, Choi H, Jeong BC, et al. Transcriptional factor ATF6 is involved in odontoblastic differentiation. *J Dent Res*. 2014;93:483-489.
7. Fei L, Chen H, Ma L, et al. Systematic identification of cell-fate regulatory programs using a single-cell atlas of mouse development. *Nat Genet*. 2022;54:1051-1061.
8. Acosta-Alvear D, Zhou Y, Blais A, et al. XBP1 controls diverse cell type- and condition-specific transcriptional regulatory networks. *Mol Cell*. 2007;27:53-66.
9. Reimold AM, Etkin A, Clauss I, et al. An essential role in liver development for transcription factor XBP-1. *Genes Dev*. 2000;14:152-157.
10. Masaki T, Yoshida M, Noguchi S. Targeted disruption of CRE-binding factor TREB5 gene leads to cellular necrosis in cardiac myocytes at the embryonic stage. *Biochem Biophys Res Commun*. 1999;261:350-356.
11. Lee AH, Chu GC, Iwakoshi NN, Glimcher LH. XBP-1 is required for biogenesis of cellular secretory machinery of exocrine glands. *EMBO J*. 2005;24:4368-4380.
12. Cox JS, Walter P. A novel mechanism for regulating activity of a transcription factor that controls the unfolded protein response. *Cell*. 1996;87:391-404.
13. Yanagitani K, Imagawa Y, Iwawaki T, et al. Cotranslational targeting of XBP1 protein to the membrane promotes cytoplasmic splicing of its own mRNA. *Mol Cell*. 2009;34:191-200.
14. Yanagitani K, Kimata Y, Kadokura H, Kohno K. Translational pausing ensures membrane targeting and cytoplasmic splicing of XBP1u mRNA. *Science*. 2011;331:586-589.
15. Glimcher LH, Lee AH, Iwakoshi NN. XBP-1 and the unfolded protein response (UPR). *Nat Immunol*. 2020;21:963-965.
16. Hetz C. The unfolded protein response: controlling cell fate decisions under ER stress and beyond. *Nat Rev Mol Cell Biol*. 2012;13:89-102.
17. Sriburi R, Jackowski S, Mori K, Brewer JW. XBP1: a link between the unfolded protein response, lipid biosynthesis, and biogenesis of the endoplasmic reticulum. *J Cell Biol*. 2004;167:35-41.
18. Khetchoumian K, Balsalobre A, Mayran A, et al. Pituitary cell translation and secretory capacities are enhanced cell autonomously by the transcription factor Creb3l2. *Nat Commun*. 2019;10:3960.
19. Lee AH, Heidtman K, Hotamisligil GS, Glimcher LH. Dual and opposing roles of the unfolded protein response regulated by IRE1alpha and XBP1 in proinsulin processing and insulin secretion. *Proc Natl Acad Sci USA*. 2011;108:8885-8890.
20. Lin W, Chen S, Wang Y, et al. Dynamic regulation of mitochondrial-endoplasmic reticulum crosstalk during stem cell homeostasis and aging. *Cell Death Dis*. 2021;12:794.
21. Sun JL, Li JY, Wang MJ, Song ZT, Liu JX. Protein quality control in plant organelles: current Progress and future perspectives. *Mol Plant*. 2021;14:95-114.
22. Chen P, Levy DL. Regulation of organelle size and organization during development. *Semin Cell Dev Biol*. 2023;133:53-64.
23. Dorn GW 2nd, Vega RB, Kelly DP. Mitochondrial biogenesis and dynamics in the developing and diseased heart. *Genes Dev*. 2015;29:1981-1991.
24. Cheng XT, Huang N, Sheng ZH. Programming axonal mitochondrial maintenance and bioenergetics in neurodegeneration and regeneration. *Neuron*. 2022;110:1899-1923.
25. Zhang F, Jiang L, He Y, et al. Changes of mitochondrial respiratory function during odontogenic differentiation of rat dental papilla cells. *J Mol Histol*. 2018;49:51-61.

26. Zhang F, Yang S, Jiang L, et al. Melatonin-mediated malic enzyme 2 orchestrates mitochondrial fusion and respiratory functions to promote odontoblastic differentiation during tooth development. *J Pineal Res*. 2023;74:e12865.
27. Lin H, Liu H, Sun Q, Yuan G, Zhang L, Chen Z. Establishment and characterization of a tamoxifen-mediated reversible immortalized mouse dental papilla cell line. *In Vitro Cell Dev Biol Anim*. 2013;49:114-121.
28. Tao H, Lin H, Sun Z, et al. Klf4 promotes Dentinogenesis and odontoblastic differentiation via modulation of TGF-β signaling pathway and interaction with histone acetylation. *J Bone Miner Res*. 2019;34:1502-1516.
29. Lin Y, Xiao Y, Lin C, et al. SALL1 regulates commitment of odontoblast lineages by interacting with RUNX2 to remodel open chromatin regions. *Stem Cells*. 2021;39:196-209.
30. Bolger AM, Lohse M, Usadel B. Trimmomatic: a flexible trimmer for Illumina sequence data. *Bioinformatics*. 2014;30:2114-2120.
31. Langmead B, Salzberg SL. Fast gapped-read alignment with bowtie 2. *Nat Methods*. 2012;9:357-359.
32. Ramírez F, Ryan DP, Grüning B, et al. deepTools2: a next generation web server for deep-sequencing data analysis. *Nucleic Acids Res*. 2016;44:W160-W165.
33. Zhang Y, Liu T, Meyer CA, et al. Model-based analysis of ChIP-Seq (MACS). *Genome Biol*. 2008;9:R137.
34. Ross-Innes CS, Stark R, Teschendorff AE, et al. Differential oestrogen receptor binding is associated with clinical outcome in breast cancer. *Nature*. 2012;481:389-393.
35. McLean CY, Bristor D, Hiller M, et al. GREAT improves functional interpretation of cis-regulatory regions. *Nat Biotechnol*. 2010;28:495-501.
36. Heinz S, Benner C, Spann N, et al. Simple combinations of lineage-determining transcription factors prime cis-regulatory elements required for macrophage and B cell identities. *Mol Cell*. 2010;38:576-589.
37. Bray NL, Pimentel H, Melsted P, Pachter L. Near-optimal probabilistic RNA-seq quantification. *Nat Biotechnol*. 2016;34:525-527.
38. Pimentel H, Bray NL, Puente S, Melsted P, Pachter L. Differential analysis of RNA-seq incorporating quantification uncertainty. *Nat Methods*. 2017;14:687-690.
39. Tripathi S, Pohl MO, Zhou Y, et al. Meta- and orthogonal integration of influenza "OMICs" data defines a role for UBR4 in virus budding. *Cell Host Microbe*. 2015;18:723-735.
40. Wang S, Sun H, Ma J, et al. Target analysis by integration of transcriptome and ChIP-seq data with BETA. *Nat Protoc*. 2013;8:2502-2515.
41. Xiao Y, Lin YX, Cui Y, et al. Zeb1 promotes odontoblast differentiation in a stage-dependent manner. *J Dent Res*. 2021;100:648-657.
42. Havalová H, Ondrovičová G, Keresztesová B, et al. Mitochondrial HSP70 chaperone system-the influence of post-translational modifications and involvement in human diseases. *Int J Mol Sci*. 2021;22:8077.
43. Shan Y, Cortopassi G. Mitochondrial Hspa9/Mortalin regulates erythroid differentiation via iron-sulfur cluster assembly. *Mitochondrion*. 2016;26:94-103.
44. Yuan M, Gong M, He J, et al. IP3R1/GRP75/VDAC1 complex mediates endoplasmic reticulum stress-mitochondrial oxidative stress in diabetic atrial remodeling. *Redox Biol*. 2022;52:102289.
45. Li J, Qi F, Su H, et al. GRP75-faciliated mitochondria-associated ER membrane (MAM) integrity controls cisplatin-resistance in ovarian cancer patients. *Int J Biol Sci*. 2022;18:2914-2931.
46. Cilleros-Holgado P, Gómez-Fernández D, Piñero-Pérez R, et al. mtUPR modulation as a therapeutic target for primary and secondary mitochondrial diseases. *Int J Mol Sci*. 2023;24:1482.
47. Pfanner N, Warscheid B, Wiedemann N. Mitochondrial proteins: from biogenesis to functional networks. *Nat Rev Mol Cell Biol*. 2019;20:267-284.
48. Chan DC. Mitochondrial dynamics and its involvement in disease. *Annu Rev Pathol*. 2020;15:235-259.
49. Harding HP, Zhang Y, Zeng H, et al. An integrated stress response regulates amino acid metabolism and resistance to oxidative stress. *Mol Cell*. 2003;11:619-633.
50. Jana S, Brahma S, Arora S, et al. Transcriptional-translational conflict is a barrier to cellular transformation and cancer progression. *Cancer Cell*. 2023;41:853-870.e813.
51. Yung HW, Hemberger M, Watson ED, et al. Endoplasmic reticulum stress disrupts placental morphogenesis: implications for human intrauterine growth restriction. *J Pathol*. 2012;228:554-564.
52. Yung HW, Colleoni F, Dommett E, et al. Noncanonical mitochondrial unfolded protein response impairs placental oxidative phosphorylation in early-onset preeclampsia. *Proc Natl Acad Sci USA*. 2019;116:18109-18118.
53. Senft D, Ronai ZA. UPR, autophagy, and mitochondria crosstalk underlies the ER stress response. *Trends Biochem Sci*. 2015;40:141-148.
54. Haynes CM, Ron D. The mitochondrial UPR - protecting organelle protein homeostasis. *J Cell Sci*. 2010;123:3849-3855.
55. Fiorese CJ, Schulz AM, Lin YF, Rosin N, Pellegrino MW, Haynes CM. The transcription factor ATF5 mediates a mammalian mitochondrial UPR. *Curr Biol*. 2016;26:2037-2043.
56. Melber A, Haynes CM. UPR(mt) regulation and output: a stress response mediated by mitochondrial-nuclear communication. *Cell Res*. 2018;28:281-295.
57. Aryal YP, Lee ES, Kim TY, et al. Stage-specific expression patterns of ER stress-related molecules in mice molars: implications for tooth development. *Gene Expr Patterns*. 2020;37:119130.
58. Fan Y, Simmen T. Mechanistic connections between endoplasmic reticulum (ER) redox control and mitochondrial metabolism. *Cells*. 2019;8:1071.
59. Giorgi C, Marchi S, Pinton P. The machineries, regulation and cellular functions of mitochondrial calcium. *Nat Rev Mol Cell Biol*. 2018;19:713-730.
60. Szabadkai G, Bianchi K, Várnai P, et al. Chaperone-mediated coupling of endoplasmic reticulum and mitochondrial Ca^{2+} channels. *J Cell Biol*. 2006;175:901-911.
61. Lee S, Wang W, Hwang J, Namgung U, Min KT. Increased ER-mitochondria tethering promotes axon regeneration. *Proc Natl Acad Sci USA*. 2019;116:16074-16079.
62. Chandrasekaran K, Najimi N, Sagi AR, et al. NAD(+) precursors repair mitochondrial function in diabetes and prevent experimental diabetic neuropathy. *Int J Mol Sci*. 2022;23;4887.
63. Zhou Z, Lu J, Yang M, et al. The mitochondrial unfolded protein response (UPR(mt)) protects against osteoarthritis. *Exp Mol Med*. 2022;54:1979-1990.

64. Romani M, Sorrentino V, Oh CM, et al. NAD(+) boosting reduces age-associated amyloidosis and restores mitochondrial homeostasis in muscle. *Cell Rep*. 2021;34:108660.

SUPPORTING INFORMATION

Additional supporting information can be found online in the Supporting Information section at the end of this article.

How to cite this article: Huang D, Li Y, Han J, Zuo H, Liu H, Chen Z. *Xbp1* promotes odontoblastic differentiation through modulating mitochondrial homeostasis. *The FASEB Journal*. 2024;38:e23600. doi:10.1096/fj.202400186R